Numerical Methods in Civil Engineering, 9-3 (2025) 47-62

Numerical Methods in Civil Engineering

Journal Homepage: https://nmce.kntu.ac.ir

Seismic resilience optimization of urban transportation network during emergency medical response: A case study in Tehran metropolis

Yaser Hosseini*, Reza Karami Mohammadi**

ARTICLE INFO

RESEARCH PAPER

Article history:
Received:
September 2024
Revised:
January 2025
Accepted:
March 2025

Keywords:
Seismic resilience
Emergency response
Road blockage
Debris evacuation
Transportation network
Road network recovery

Abstract:

Urban pathways play a critical role in the functionality and safety of cities, especially during and after seismic events. Earthquakes, by their very nature, pose significant risks to urban infrastructure, often resulting in the collapse of buildings and the subsequent blockage of roads and pathways. The resilience of these urban pathways is crucial for ensuring that emergency services can reach affected areas, that evacuation routes remain open, and that the city can recover quickly from the disaster. This paper explores the seismic resilience of urban pathways, focusing on the challenges posed by building debris and the strategies needed to mitigate these risks. Understanding and enhancing the resilience of these pathways is crucial for decreasing the impact of earthquake on populations and infrastructure. In network restoration planning, various uncertainties have been accounted for by probabilistic models to calculate the average of pathways recovery time. To evaluate network performance after an earthquake, a network functionality index has been suggested. A Simulated Annealing-based framework is developed to maximize resilience. The optimization algorithm gives the maximum amount of needed resources and the optimal order of network recovery. The suggested approach is applied to Region 2 of the Tehran metropolitan area. According to the optimization results, the 10 resources can unblock the transportation network within predefined goal times. Also, the findings show that as the amount of resources increases, the influence of resources on decreasing network completion time diminishes.

1. Introduction

In urban environments, the resilience of transportation networks is crucial for ensuring a prompt response and recovery in the aftermath of seismic events. Earthquakes can lead to the collapse of buildings, resulting in the blockage of roads and hindering emergency response efforts, evacuation procedures, and post-disaster recovery. Understanding the mechanism of urban road obstruction caused by falling building debris and devising effective strategies for restoring transportation networks are imperative for mitigating the impact of earthquakes on urban communities.

Many instances of roadside structure collapses causing route obstructions during previous large earthquakes have been documented [1].

The primary cause of post-earthquake traffic blockage in metropolitan areas is the collapse of buildings near the paths [2], which may greatly impact the speed of emergency services responses [3]. Therefore, the prediction of road blockage resulting from building collapses during earthquakes is a critical step in disaster preparedness and response planning. By accurately forecasting the areas most likely to be affected by road blockages, emergency responders can strategize their efforts and allocate resources efficiently, potentially saving lives and minimizing disruptions to essential services.

Establishing an emergency restoration strategy and forecasting the state of the road obstruction caused by building collapses are challenging due to uncertainty. This work uses probabilistic models to address this issue, explicitly accounting for various uncertainties such as earthquake magnitude, rupture locations of fault, seismic intensity, building damage, debris width, blockage conditions, debris volume, and the uncertainty in debris evacuation rates.

** Ph.D. in Earthquake Engineering, Department of Civil Engineering, K. N. Toosi University of Technology, Tehran, Iran. Email: hosseini@email.kntu.ac.ir*

*** Corresponding author: Associate Professor, Department of Civil Engineering, K. N. Toosi University of Technology, Tehran, Iran. Email: rkarami@kntu.ac.ir*

https://doi.org/10.61186/NMCE.2409.1075

There is limited research on traffic blockages caused by falling building debris after an earthquake. Existing research does not address network recovery after the blockage; instead, it only predicts the route "vulnerability" [4,5], "blockage probability" [6,7], or "network performance degradation" [8,9] due to falling building debris.

Only theoretical models have been developed for network recovery planning in certain Operations Research studies. These models were created employing Graph Theory [10–12] and Linear Programming Methods [13–16], usually without doing a comprehensive obstruction assessment and with hypothetical recovery times. Network blockage evaluation and network recovery strategy must be taken into account continuously in an exhaustive framework since this has not been done in the literature. Predicting the quantity of debris and the time needed to clear each obstructed route is necessary to offer network restoration plans. Since system recovery planning is the objective, "restoration time" has to be calculated. Using the mean value of debris volume and debris removal rate, we compute the mean recovery time for every route in this study. Within our technique, the anticipated values of the critical reconnection time courses feed an optimization algorithm that determines the necessary resources and the best order of recovery activities.

The main objective of the research is to fill the gap between i) anticipating transportation network obstruction, ii) optimizing resource allocation for network recovery planning, and iii) maximizing network resilience in the medical reaction stage.

The remaining sections of the study are organized as follows: Section 2 outlines the definition of the Resilience Factor. Section 3 describes the interdependent probabilistic models to predict the mean time to evacuate a blocked route. In Section 4 the emergency functionality index of the network is proposed. Section 5 develops an algorithm to solve the optimization model. Section 6 provides a case study, and section 7 is the conclusion of this study.

2. Resilience Factor

In past years, the notion of resilience has emerged as a pivotal concept in various fields, ranging from disaster management to organizational psychology [17]. One of the seminal contributions to this discourse comes from Bruneau et al. [18], whose definition of seismic resilience provides an exhaustive basis for conceptualizing resilience in the face of seismic events. As outlined in the concept by Bruneau et al. [18], seismic resilience is the capacity of the system to return to normal performance in the shortest possible time. Key aspects include robustness, resourcefulness, redundancy, and rapidity to guarantee the system can withstand and quickly restore from seismic events [19,20]. **Robustness:** This dimension focuses on the system's capability to withstand extreme events. It evaluates the structure and infrastructure stability, as well as the resilience of social and economic systems. A robust system can resist damage and maintain functionality even when faced with significant stressors.

Rapidity: rapidity refers to the speed and efficiency of the restoration process following a seismic event. It assesses how quickly essential services can be restored, damaged infrastructure repaired, and disrupted activities resumed. A rapid response is crucial for minimizing the impact of disasters and facilitating swift recovery.

Resourcefulness: resourcefulness highlights the ability to mobilize and allocate resources effectively for system restoration. This dimension evaluates the availability of financial, human, and material resources, as well as the efficiency of resource management mechanisms. Resourcefulness ensures that necessary resources are promptly deployed to support recovery efforts and address critical needs.

Redundancy: redundancy pertains to the presence of alternative or backup systems/components that can fulfill essential functions during extreme events. It assesses the degree of redundancy built into infrastructure, systems, and processes to ensure continuity of operations in the face of disruptions. Redundancy minimizes vulnerabilities by providing fallback options and enhancing system resilience. Various analytical relationships have been introduced for quantifying resilience [21-23]. A well-known quantitative resilience indicator that is generated from the functionality recovery trajectory is used in this investigation [24,25]. Eq. (1) presents the seismic resilience index (RI) derived from the functionality-time curve:

$$Resilience = \frac{\int_{t_0}^{t_f+T_{RE}} Q(t)dt}{T_{RE}} \quad (1)$$

Q (t) denotes the network functionality that is reliant on time, the beginning moment of network restoration is indicated by t_0, $t_f + T_{RE}$ signifies the finishing moment of restoration, and T_{RE} is the restoration period, as illustrated in Figure 1.

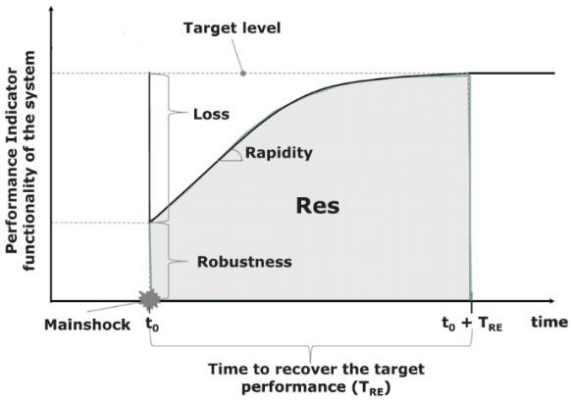

Fig. 1: Diagrammatic depiction of resilience.

3. Probabilistic Models

The probabilistic models method has been utilized to characterize resilience evaluation uncertainties. Mahsuli and Haukaas initially introduced the probabilistic model's procedure in earthquake risk evaluation using reliability techniques [26]. Using the mentioned approach, every source of uncertainty is simulated as a separate random variable. The advantage of the probabilistic models approach is that random variables explicitly model sources of uncertainty unlike implicit modeling of uncertainty through conditional probability models [27].

Probabilistic models such as Magnitude, Rupture Location, Intensity, Damage, Debris, Blockage, and Evacuation models have been used in this article. Figure 2 illustrates the flowchart of probabilistic models. Random parameters are input into the models, each of which generates an array of outputs which are then used as inputs for the subsequent model. Below is a brief overview of the probabilistic models, which are described in detail in our recent studies [28,29]. The parameters of the probabilistic models in Fig. 2 are explained in Table 1.

3.1. Magnitude model: Takes into account the maximum magnitude (M_{max}) that a particular fault is capable of producing, depicting the most severe potential outcome.

3.2. Location model: Calculates the hypocentral distance (R_{hypo}) to different building locations based on the assumption that the rupture point distributes evenly along the fault zone.

3.3. Intensity Model: Takes magnitude and hypocenter distance as inputs and calculates PGA at the place of every structure. The basis of the intensity model is the attenuation equation for Iran developed by Darzi et al. [30].

3.4. Damage model: The damage index (DI) is the model's output, and its input parameters are PGA and the structural characteristics of the structure. Fallah Tafti et al. [31] established fragility curves for common Iranian structures that provide the damage model's basis. The damage factor is classified into five categories and varies between 0 and 4. Damage indices that are passed on to the subsequent model are those associated with complete collapse (ranging from 3 to 4).

3.5. Debris model: Employing the Argyroudis-developed debris expansion [4], [9], [32,33], this model forecasts the debris width (w_d) for a collapsed structure**.**

3.6. Blockage Model: Three types of obstruction are distinguished by this model: non-blockage, minor blockage, and complete blockage (See Ref. [28] for detailed information) and this model estimates mean debris volume $\left(E(V_d^p)\right)$ that needs to be eliminated to open the blocked path.

3.7. Evacuation Model: The mean time to evacuate a blocked route is computed using the Eq. (2):

$$E(t_E^p) = \left(\text{debris volume}/\text{removing rate}\right) \quad (2)$$

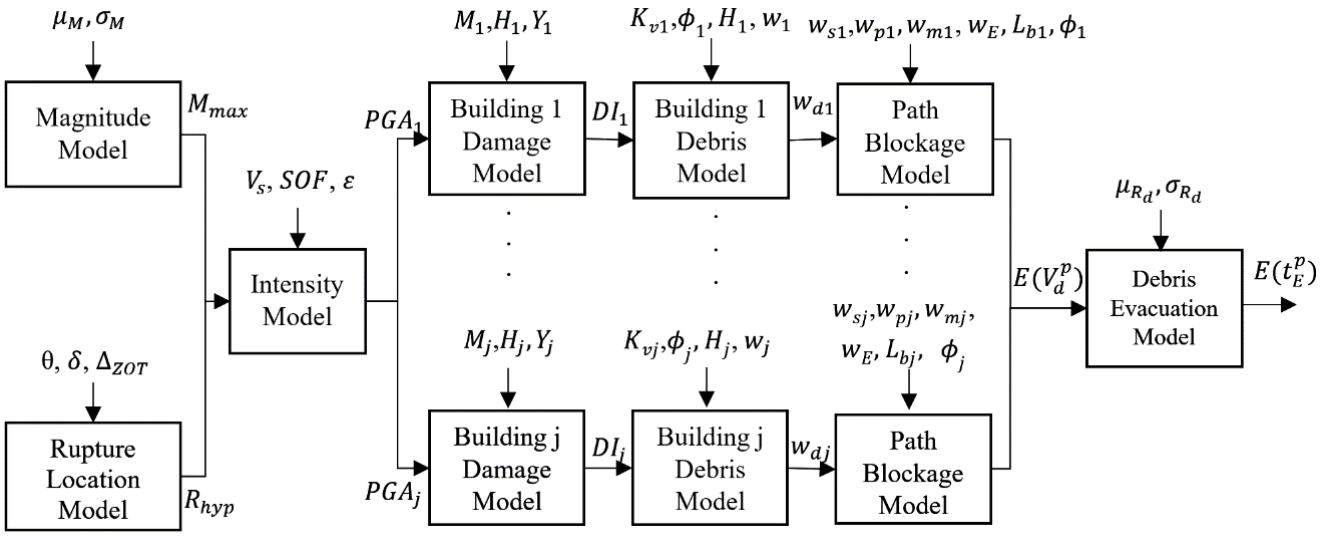

Fig. 2: Probabilistic models flowchart used for calculating the mean of required time to clear a blocked route.

Table 1: Explanation of the parameters of probabilistic models in Fig. 2.

Symbol	Description	Parameter type
μ_M & σ_M	Mean and standard deviation of maximum magnitude, respectively	Constant
M_{max}	Maximum magnitude	Random
θ	Fault location coordinates	Constant
δ	Dip angle of the fault	Constant
Δ_{ZOT}	Depth to top of the fault	Constant
R_{hyp}	Hypocentral distance	Model response
V_s	Shear wave velocities at building locations	Constant
SOF	Style-of-faulting mechanism	Constant
ε	Model error term	Random
PGA_j	Peak ground acceleration at the *j*th building site	Model response
M_j	Building j Material	Constant
H_j	Building j Height	Constant
Y_j	Building j Year built	Constant
DI_j	Building j Damage Index	Model response
ϕ_j	Building j collapse angle	Random
K_{vj}	Building j volume reduction coefficient	Random
w_j	Building j width	Constant
w_{dj}	Building j debris width	Model response
w_{pj}	Width of the *p*-th path in front of the *j*-th building	Constant
w_{sj}	Building *j*-th to path distance	Constant
w_{mj}	Middle width of path in front of the *j*-th building	Constant
w_E	Width required for emergency vehicles passage	Constant
Lb_j	Length of the *j*-th building (dimension parallel to the path)	Constant
$E(V_d^p)$	Expected value of *p*-th path emergency debris volume	Model response
μ_{R_d} & σ_{R_d}	Mean and standard deviation of resource removing rate, respectively	Constant
$E(t_E^p)$	Expected value of *p*-th path emergency debris evacuation time	Model response

4. Network functionality

The blockage of paths can severely disrupt the flow of emergency services, the transportation of essential goods, and the overall response to emergency situations. Therefore, assessing and improving the performance of networks under emergency conditions after an earthquake is a critical necessity. Eq. (3) characterizes the critical functionality of the transportation network:

$$Q(t) = \frac{[\sum_{b=1}^{B-1}\sum_{a=b+1}^{B}\delta_{ba}^{t}\times\omega_b\times(NED_b)\times\omega_a\times(NED_a)]_t}{[\sum_{b=1}^{B-1}\sum_{a=b+1}^{B}\delta_{ba}\times\omega_b\times(NED_b)\times\omega_a\times(NED_a)]_{T_{max}}} \quad (3)$$

$Q(t)$: Network functionality such that $Q(T_{max}) = 1$
$a = [1,2,\dots,b,\dots,B]$: The array of nodes
$\delta_{ab} = 1$ When node b and node a are linked, otherwise $\delta_{ab} = 0$
T_{max}: Network recovery completion time
ω_a: Distance weight of node a
NED_a: Emergency demand of node a

ω_a is computed based on the shortest distance from node a to the closest urgent node (i.e. $\min\{\mathrm{dis}_{E_1-a}, \mathrm{dis}_{E_2-a}, \mathrm{dis}_{E3-a}, \cdots \mathrm{dis}_{E_e-a}\}$) by Equation (4):

$$\omega_a = \frac{\varphi_a}{\sum_{a=1}^{A}\varphi_a}$$
$$\varphi_a = \frac{1}{\min\{dis_{E_1-a},\ dis_{E_2-a},\ dis_{E3-a},\ \cdots\ dis_{E_e-a}\}} \quad (4)$$

Where $E = \{E_1, E_2, \cdots E_e\}$ is the array of critical nodes in study area.
Normalized emergency demand of node a, NED_a, is determined by the emergency demand in the district.
The assumption is that the need for emergency aid in a district is linked to the level of building damage and the population size of the district. Equation (5) assesses the overall emergency demand of the district instead of focusing on the damage to individual buildings.

$$(DED_d) \propto \left(\sum_{bt=1}^{BT}\rho_{bt}\times DI_{bt}\,|\,PGA_{(district\ center)}\right)_d \times (PoP)_d \quad (5)$$

DED_d: The need of d-th district for emergency aid
ρ_{bt} : The proportion for every specific building type within district
DI_{bt}: The damage index for the building type (bt)
$(PoP)_d$: The district's (d-th) population
Equation (6) converts district emergency demand into nodal emergency demand, as shown below:

$$NED_a = \sum_{d}^{D} \frac{(DED_d)}{N_d} \quad (6)$$

NED_a: The u-th node's emergency the demand
N_d: The whole node count in the vicinity of district (d)
D: The quantity of districts that are linked to node u

5. Optimization of network restoration

The goal of optimization is to identify the quantity of resources needed during the medical response stage, determine the most efficient order of routes unblocking, and calculate the time that each task should begin and end. The optimization approach, outlined in the flowchart of Figure 3, is developed using the Simulated Annealing (SA) algorithm.

The decision variables in this study include the number of required resources (Rmax), the optimal task sequence for each resource (χ(r)), the start and finish times of each task (ST(r), FT(r)), and the prioritized pathways for restoration to optimize network resilience and minimize network total restoration time.

The optimization constraints and assumptions are:
1) The restoration operation starts from the emergency node. 2) The operation is carried out by a limited number of resources and each resource can handle one blocked road in a moment. 3) The travel times of resources between restoration tasks are ignored because restoration times are much longer than travel times. 4) The resource units cannot traverse debris-blocked roads, i.e., for a resource to reach a debris-blocked edge; there needs to be a cleared path to the path from the resource's current location. In other words, a task can start when all the predecessors have already been done. A brief explanation of each step in the optimization flowchart is given in Figure 3.

Step 1: Information on the emergency stage and the topology of the network is acquired, and the optimization process receives input from probabilistic models.

Step 2: A shortest path tree (SPT) is generated using the emergency nodes as the reference points, and the restoration efforts are organized into three priority levels. The emergency shortest path tree (ESPT) constitutes a subset of the graph that includes all emergency nodes, characterized by the lowest weight and the fewest possible number of links. Dijkstra's approach [34] is used to generate the ESPT, and the edge weights, or pathways, are specified in Eq. (7):

$$LW_{ab} = \frac{1}{\omega_a \times \omega_b \times (NED_a) \times (NED_b)} \quad (7)$$

LW_{ab}: The weight of the route between nodes a and b.
Routes restoration is organized within three levels, guided by the ESPT. At the initial level, the ESTP paths with direct connections to urgent nodes should be reinstated. In the next stage, the remaining routes of the ESPT are restored, and at the final level, the recovery of the rest of the network's paths must be done. The recovery in three levels creates what is known as predecessor array, referred to as 'Pred List' or (PL) in Figure 3. The PL dictates that an obstructed route must be reinstated just after all its preceding paths are unblocked.

Step 3: Random order for restoring the obstructed route is created and represented as the (q).

Step 4: Using the PL along with a repair mechanism, the (q) is converted to a feasible sequence (p).

Step 5: For the r-th resource, the tasks (**χ(r)**) and their order, Starting Time (ST(r)) and Finishing Time (FT(r)) are defined. Resources are allocated based on constraints (8-12) as follows:

$$\sum_{t}(UR(t) + RR(t)) = R_{max} \quad (8)$$

$$t_{1p} = ST_p \geq max\{FT_z | z \in PredList(p)\} \quad (9)$$

$$t_{2p} = ST_p \geq min\{t | (RR(t + E(t_E^p)) \geq 1\} \quad (10)$$

$$ST_p^r = \max(t_{1p}, t_{2p}) \quad (11)$$

$$FT_p^r = ST_p^r + E(t_E^p)) \quad (12)$$

UR: Utilized Resources
RR: Remaining Resource
R_{max}: Maximum available resources
ST_p: p-th work start time
ST_p^r: p-th work of r-th resource start time
FT_p^r: p-th work of r-th resource finish time
$E(t_E^p))$: mean of *pth* route unblocking duration.
Constraint (8) states that the sum of the Used Resources (UR) and Remaining Resources (RR) is equal to the maximum available resources (R_{max}), at any time. Constraint (9) satisfies the predecessor time relations and states that the start time of the p-th task (ST_p) must be greater than all its predecessor tasks' finish time (FT_z). Constraint (10) gives the first time that the resource is available to start and finish the p-th task. In Constraint (10), $E(t_E^p)$ represents the duration of the p-th task according to Section 3.7. Start time for the p-th task of the r-th resource (ST_p^r) and its corresponding finish time is determined by Equations (11) and (12).

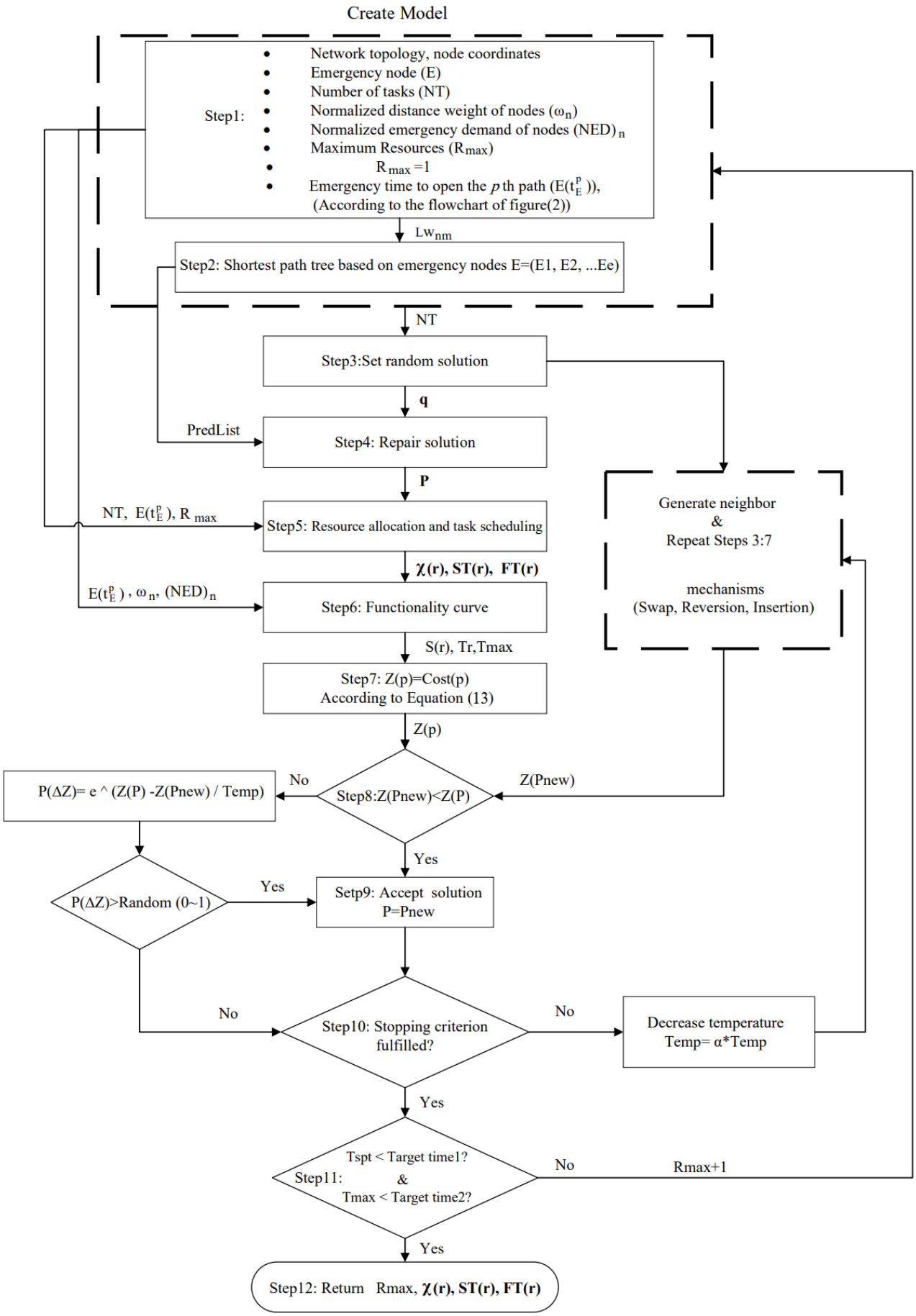

Fig. 3: Flowchart of the proposed algorithm utilizing the Simulated Annealing method.

Step 6: For each resource, a stepwise functionality curve is created and the loss of resilience (S'(r)) is computed.

Step 7: The objective function of this study, as outlined in Equation (13), is to minimize the total network restoration time (T_{max}) and resilience loss, $S'(r)$. It can be achieved by optimizing resource allocation and task sequencing.

$$Z = min\left[c.T_{max} + (1-c)\sum_{r=1}^{Rmax}\overbrace{\left(1\times T_r - S(r)\right)}^{S'(r)}\right] \quad (13)$$

$T_{max} = max\{T_r | r = 1 \dots R_{max}\}$
$c \in [0,1]$: Weighting factor
$S'(r)$: Resilience loss area for r-th resource

Steps 8 and 9: A new solution, denoted as (P_{new}), is created, and its associated cost is calculated using Equation (13). This new solution is generated through the use of three different techniques: (a) Swap, (b) Reversion, and (c) Insertion. If $Z(P_{new}) < Z(P)$, then P_{new} is immediately selected as the best candidate for restoration order. If $Z(P_{new}) > Z(P)$, then P_{new} is evaluated using an alternative acceptance criterion based on the Boltzmann probability distribution, as described in Eq. (14):

$$p(\Delta Z) = e^{\frac{Z(P)-Z(P_{new})}{T_{emp}}} \quad (14)$$

T_{emp}: The heat in the refrigeration process
The P_{new} is considered the optimal one if $p(\Delta Z)$ exceeds a randomly generated number between 0 and 1.

Step10: The iterative process is concluded when the change between two successive iterations, denoted as δe, meets a predefined threshold, serving as the termination criterion $0 < \delta e < 0.01$.

Step11: Two goals have been established for recovery: TargetTime 1 focuses on recovering the ESPT, while TargetTime 2 aims to restore the network completely.
The requirements of Eq. (15) must be satisfied in order to determine the number of resources needed for recovery:

$$T_{Espt} < TargetTime\ 1 \quad \& \quad T_{max} < TargetTime\ 2 \quad (15)$$

T_{Espt} : ESPT recovery time
T_{max} : Total network recovery time

Step 12: Step 12 provides the final results, which include the number of resources needed R_{max}, the best work order for every resource $\boldsymbol{\chi(r)}$, and the starting time (**ST(r)**) and finishing time (**FT(r)**) of works.

6. Case study

Due to its position on numerous active fault lines, Tehran is considered one of Iran's seismically active areas. North Tehran is among the main faults in this area, which have historically caused destructive earthquakes. These faults, driven by tectonic activities in the region, are prone to generating major earthquakes, posing significant risks to Tehran and its surrounding areas. Given the high population density and extensive construction in Tehran, the occurrence of severe earthquakes could result in substantial human and financial losses. Therefore, seismic resilience studies are of critical importance in this city. For this research, Region 2 of Tehran has been chosen as the focus of the case study with a population of 620,000. Figure 4 provides a detailed view of the route network analyzed in this research. As illustrated in Figure 4(a), this area contains a total of six hospitals. according to Figure 4(b), there are 33 districts, 51 nodes, and 81 pathways in the route network. In Figure 4(b), the road numbering is represented by yellow boxes, nodes by blue loops, and district numbering by the loop inside every district.

(4a)

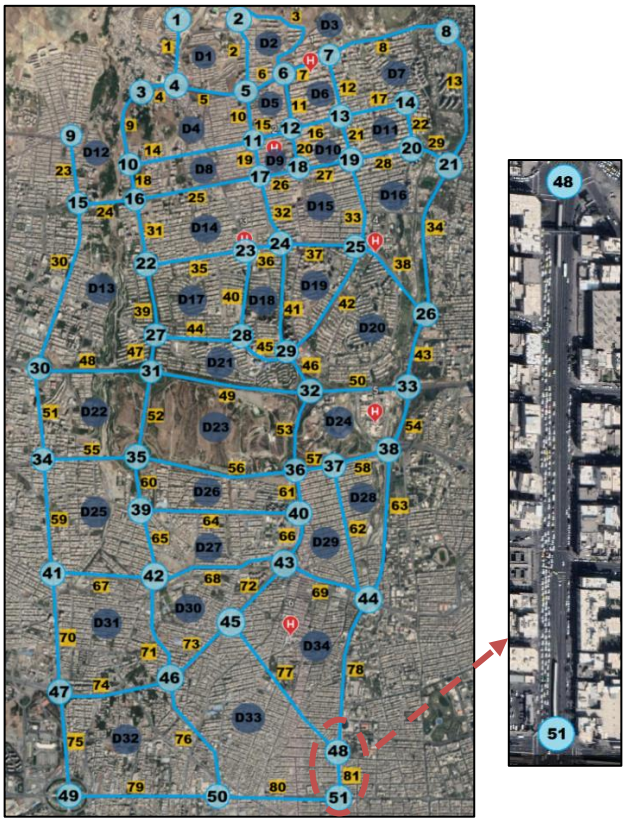

(4b) (4c)

Fig. 4: (a) Tehran's Region 2, featuring six hospitals designated as urgent nodes, (b) the network configuration, (c) a close-up view of path 81.

6.1. Probabilistic Models Calibration

As outlined in the flowchart in Figure 3, this part uses probabilistic models to determine the mean time for the opening pathways. The fundamental inputs required for fine-tuning probabilistic models include seismic source information, building characteristics, and the geometric dimensions of each path. The North Tehran fault has been determined as the seismic source affecting the road network; Figure 5 shows the geometry of the fault line.

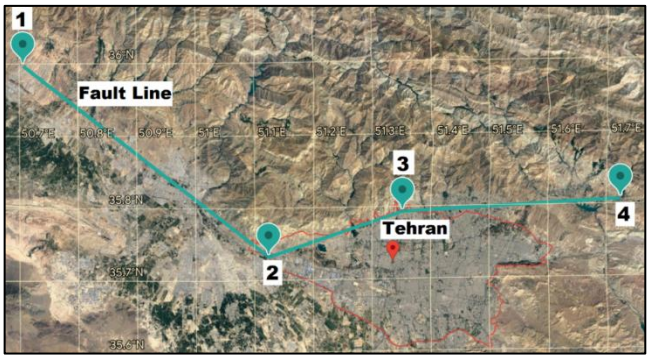

Fig. 5: The linear fault's geographic location.

Figure 6 classifies the structures in the study region according to their elevations. The input parameters of the probabilistic models outlined in Section 3 need to be specifically adjusted for the study region. Table 2 summarizes the values of the probabilistic models' parameters. In Table 2, the mean values of normal and log-normal parameters are taken from the given references.

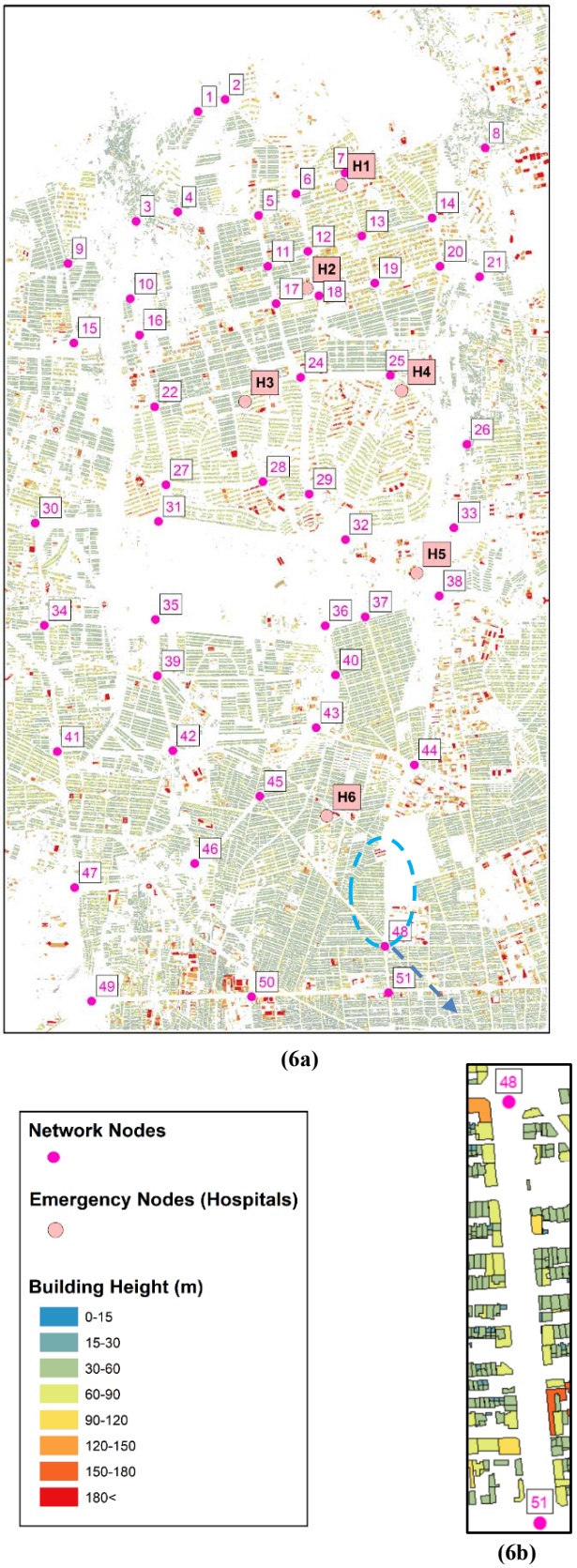

(6a) (6b)

Fig. 6: (a) Building classification by height model, (b) a close-up view of path 81 and roadside structures.

Table 2: Parameters of probabilistic models for the case study area.

Symbol	Characteristics
M_{max}	Log Normal(7.2,0.2), [35]
Δ_{zot}	2 km, [35]
δ°	75°, [35]
V_s	375-750 m/s(soil type II)
F_{SOF}	Reverse, [35]
ε	Normal $(0, 0.259)$, [30]
ϕ	Log $Normal$ $(45^{\circ}, 15^{\circ})$, [9]
k_v	Log $Normal$ (0.5,15), [9]
γ_v	1.1
R_d	Log Normal (250,50) $\frac{m^3}{hr}$, [36]

As shown in Table 2, a lognormal distribution has been considered for the path-opening rate of a resource (R_d) with a mean of 250 $\frac{m^3}{h}$ and a standard deviation of 50 $\frac{m^3}{h}$ [36]. A thorough examination is necessary to identify the makeup of a resource unit (or an emergency response team), encompassing the quantity of personnel, equipment, and materials. To reduce relevant uncertainty, a specific crisis management organization can evaluate the path-opening rate capacity of its available resources (in the preparation stage) and change the mean and standard deviation following the capacity of its own resources.

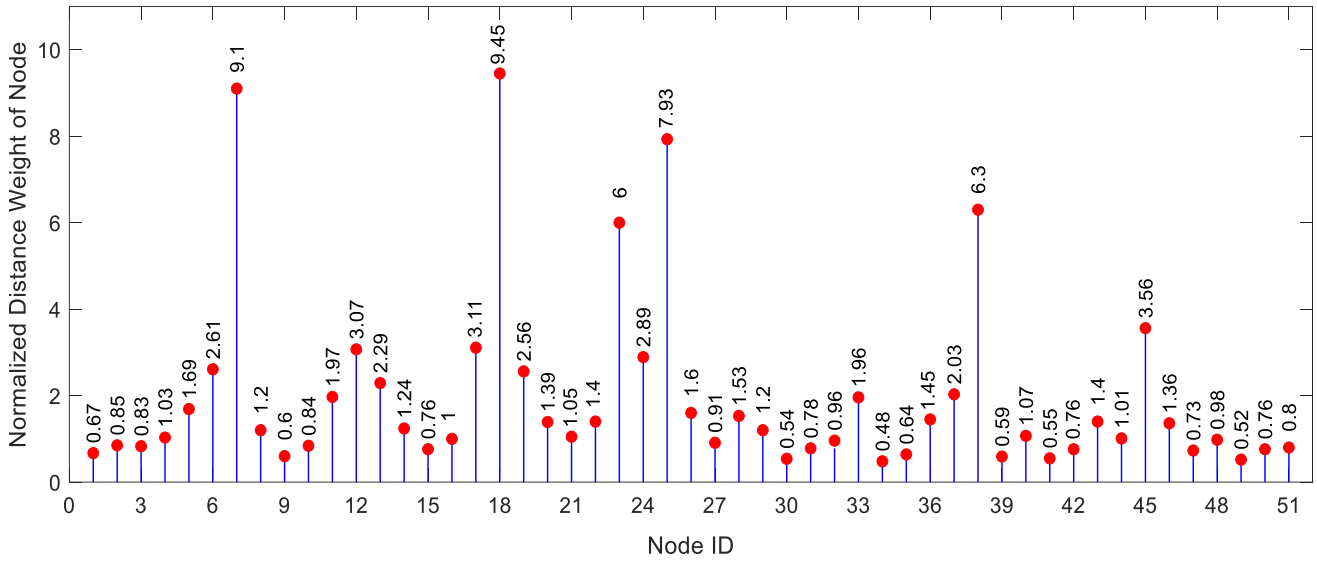

Fig. 7: Values of (ω).

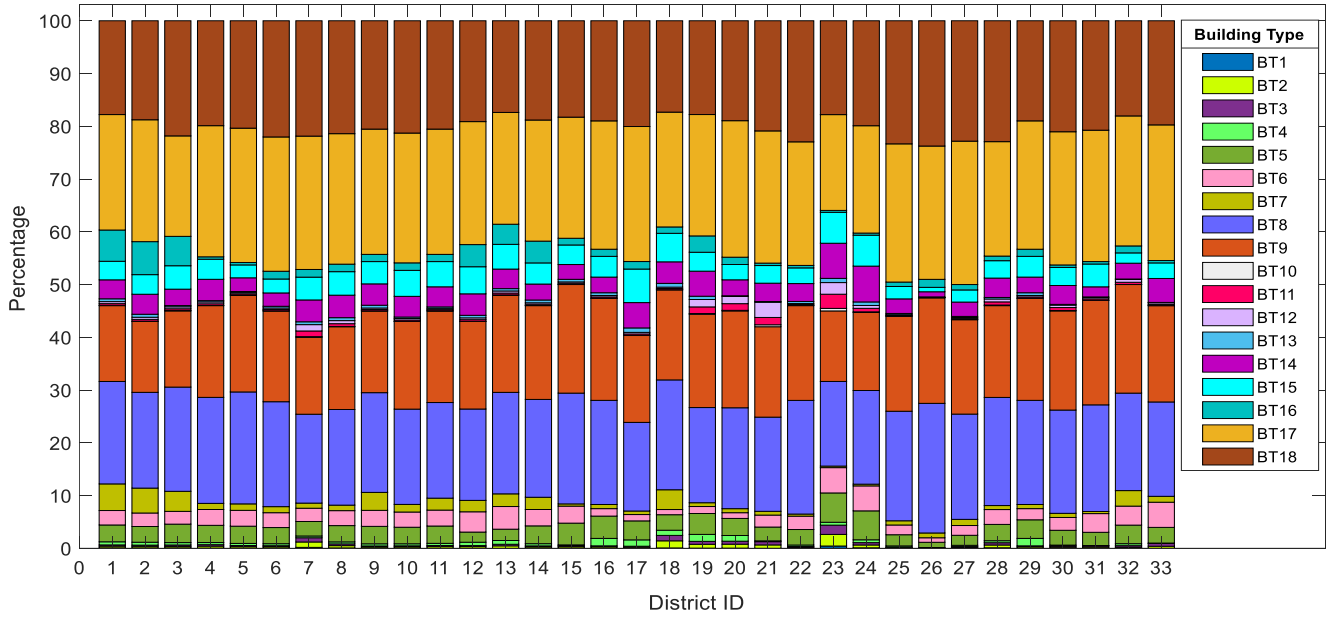

Fig. 8: Values of (ρ_{bt}).

6.2. Optimizing the recovery of network

This research examines the maximum potential magnitude that the North Tehran fault could produce, specifically $M_{max} = 7.2$, as outlined in Table 2. According to the optimization process illustrated in Figure 3, step (1) requires calculating the (ω) and (NED) for the nodes, respectively. Figure 7 presents (ω) value for each node, computed as described in Section 4.

In order to calculate NED using Equations (5) and (6), it's essential to identify the percentage of each structure type in every district (ρ_{bt}) and determine the population of that district $(PoP)_d$. Figure 8 shows the value of ρ_{bt}, and Figures 9 and 10 display the population count for each district and the categorization of population blocks respectively. Figure 11 demonstrates the NED values for the nodes.

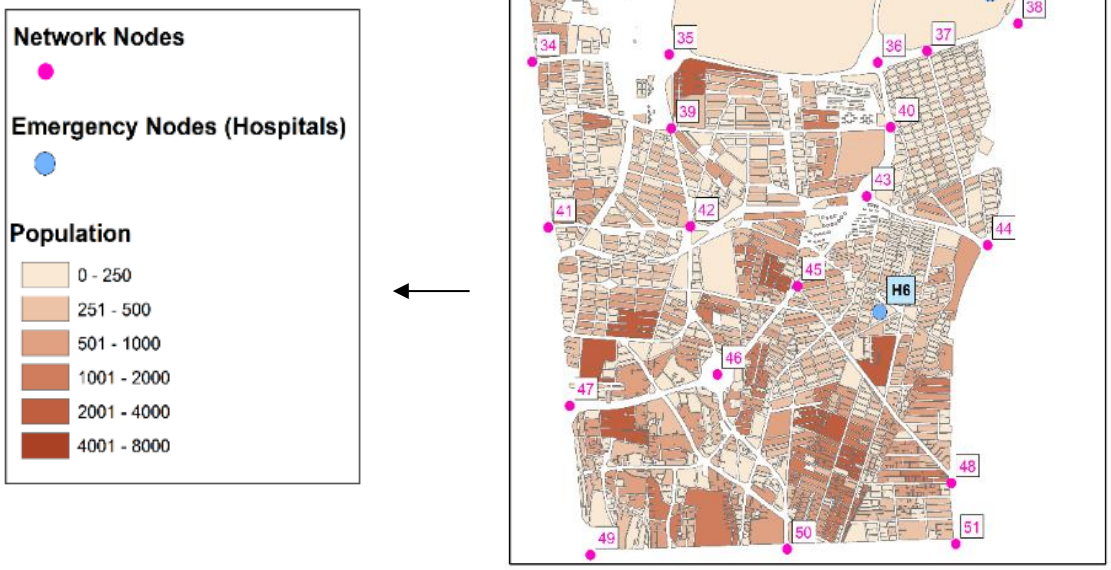

Fig. 10: Population block categorization within the study region.

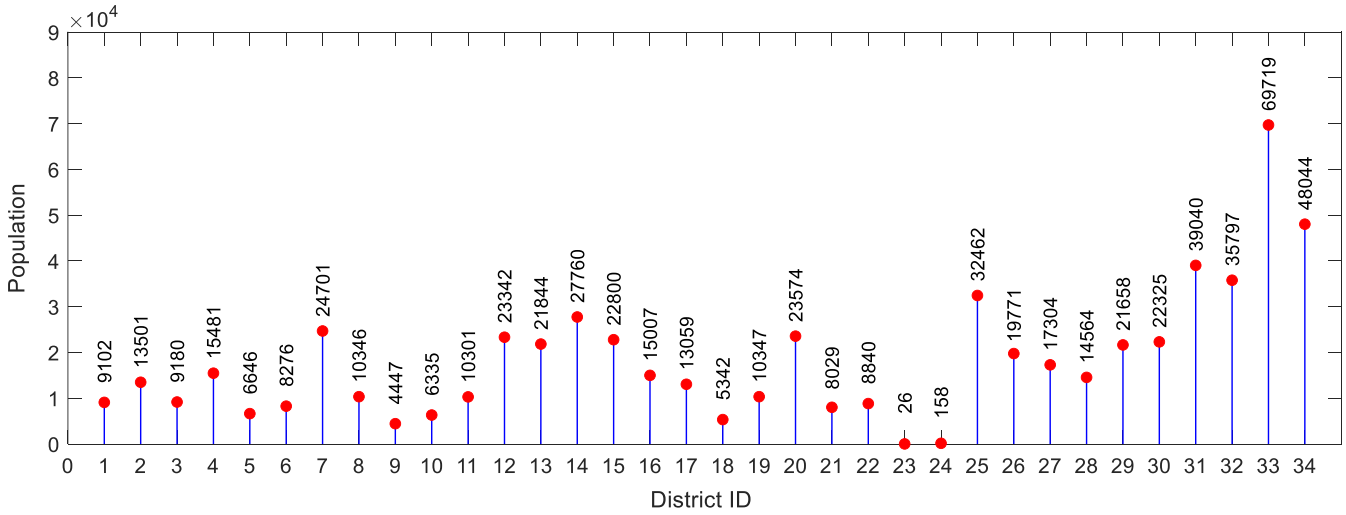

Fig. 9: Values of $(PoP)_d$.

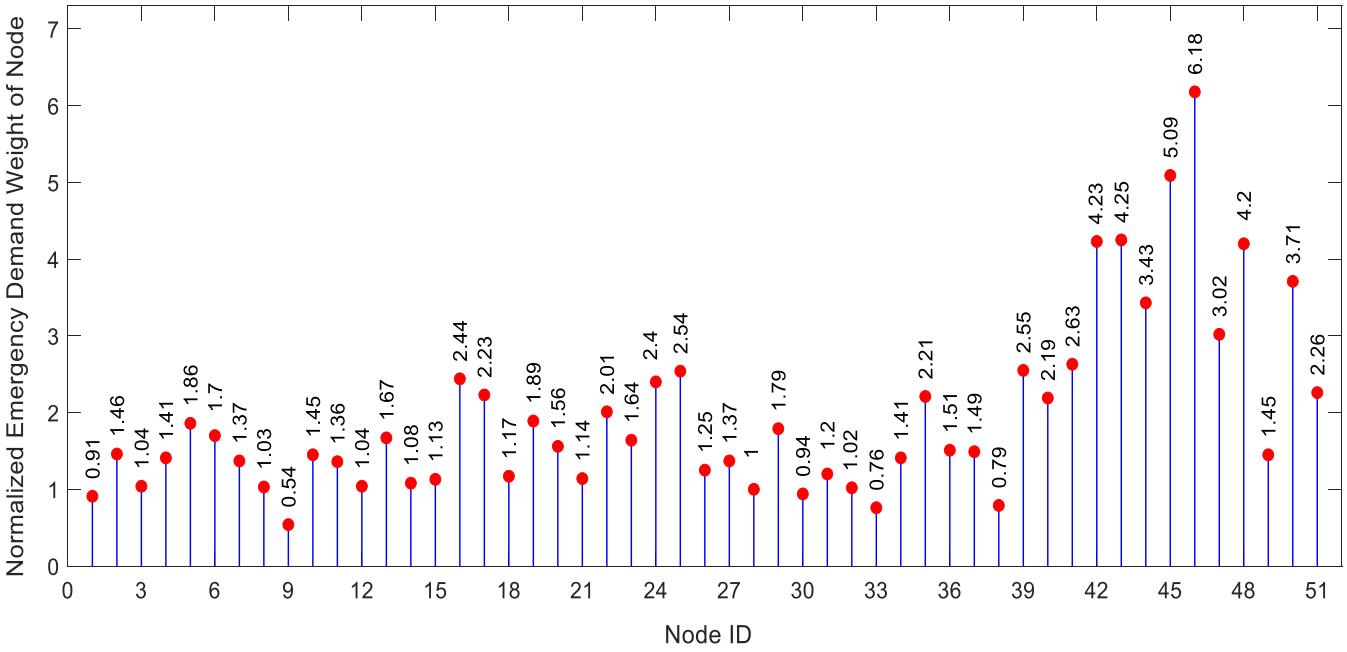

Fig. 11: The values of NED.

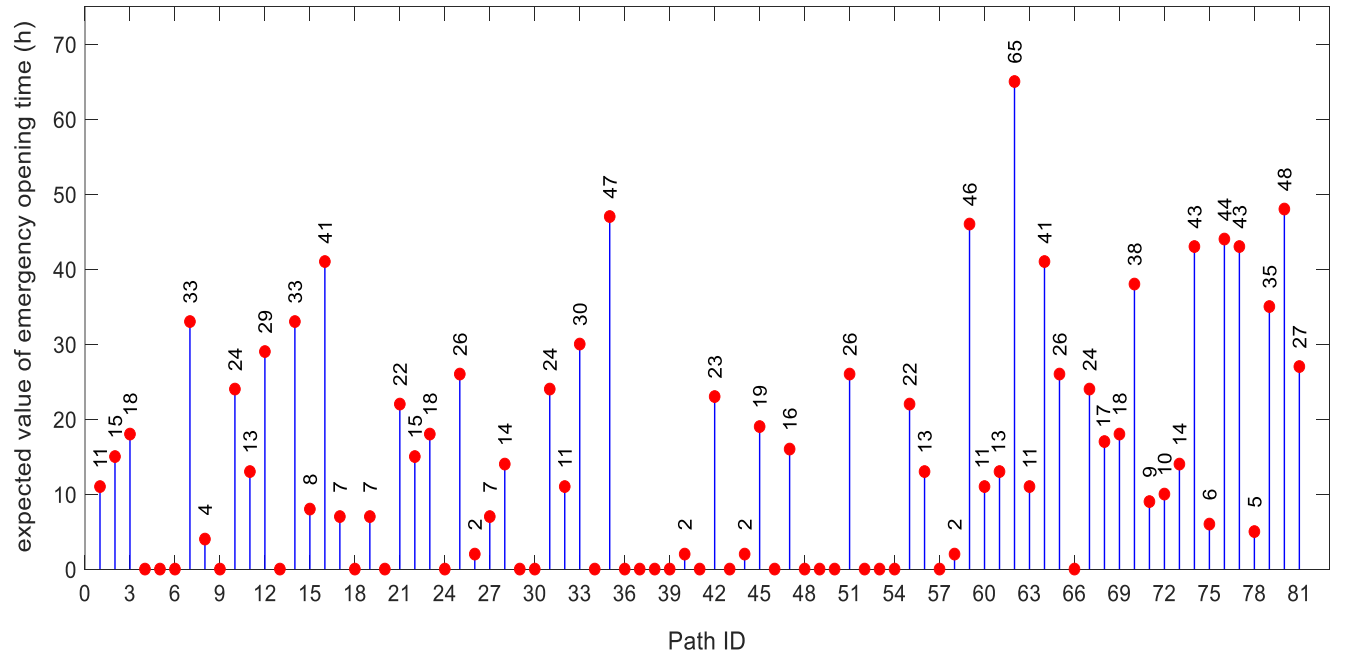

Fig.12: The mean of unblocking duration for routes $E(t_E^p)$.

As outlined in step (2) of Figure 3, the ESPT that includes urgent nodes should be identified to create the PL for network recovery. The ESPT obtained using the Dijkstra method and edge weights from Equation (7) is shown in Figure 13. There are three different levels involved in the network recovery procedure, as shown in Figure 13. In the initial level (highlighted in red), the routes of the ESPT that are linked to the urgent nodes should be opened. The remaining ESPT segments are reinserted in the second level, and the residue of routes is opened in the third level.

Table 3 lists the precise tuning parameters used during the optimization process, and Figure 14 shows the optimization's outcomes.

As shown in Figure 14(c), when 10 resources are available ($R_{max} = 10$), the values for T_{spt} and T_{max} are 79 hours and 118 hours, respectively. Both of these times are shorter than Target Times 1 = 80h and Target Times 2 = 120h. Thus, using 10 resources ($R_{max} = 10$) satisfies the resilience aim.

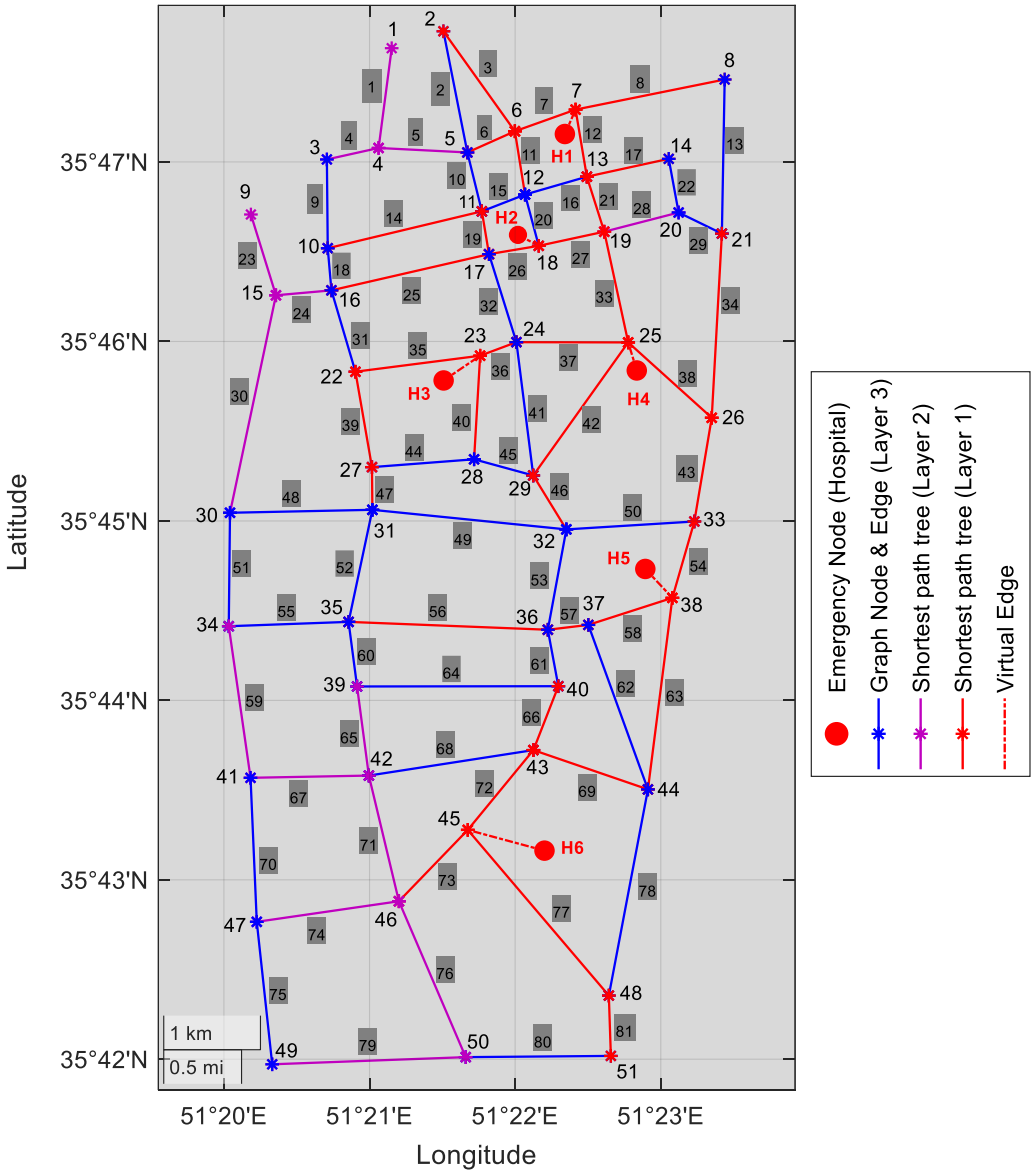

Fig. 13: The ESPT that includes urgent nodes.

Table 3: Parameters for optimization.

Symbol	Description	value
NB	Number of blocked paths	55
C	The weighting factor of the cost function	0.6
$(T_{emp})_0$	Initial temperature	10
α	Temperature reduction coefficient	0.98
Target Time 1	Time required to restore shortest-path tree	80h
Target Time 2	Total network restoration time	120h

Figure 14(a) shows how resource units affect the network's performance. In other words, the contribution of each resource to the network's functioning by clearing obstructed pathways at time t is represented by $Q_r(t)$ in the Figure 14(a). At the end of the functionality curves, the sum of all functionalities has to equal$1 - Q_0$. The network's remaining functionality to obstructions is reflected in the term Q_0, which denotes its post-earthquake robustness. There are 26 unobstructed pathways (paths with zero opening time), indicated in Figure 12, and the sum of their functions is $Q_0 = 0.154$. Consequently, the total functionality at the end time must equal $1 - Q_0 = 0.846$.

Equivalent functionality profiles $(Q_e(t))$ are produced and shown in Figure 15 to clearly assess the influence of resource amount on network resilience. The optimal functionalities at each moment in time are summed together to generate the $Q_e(t)$.

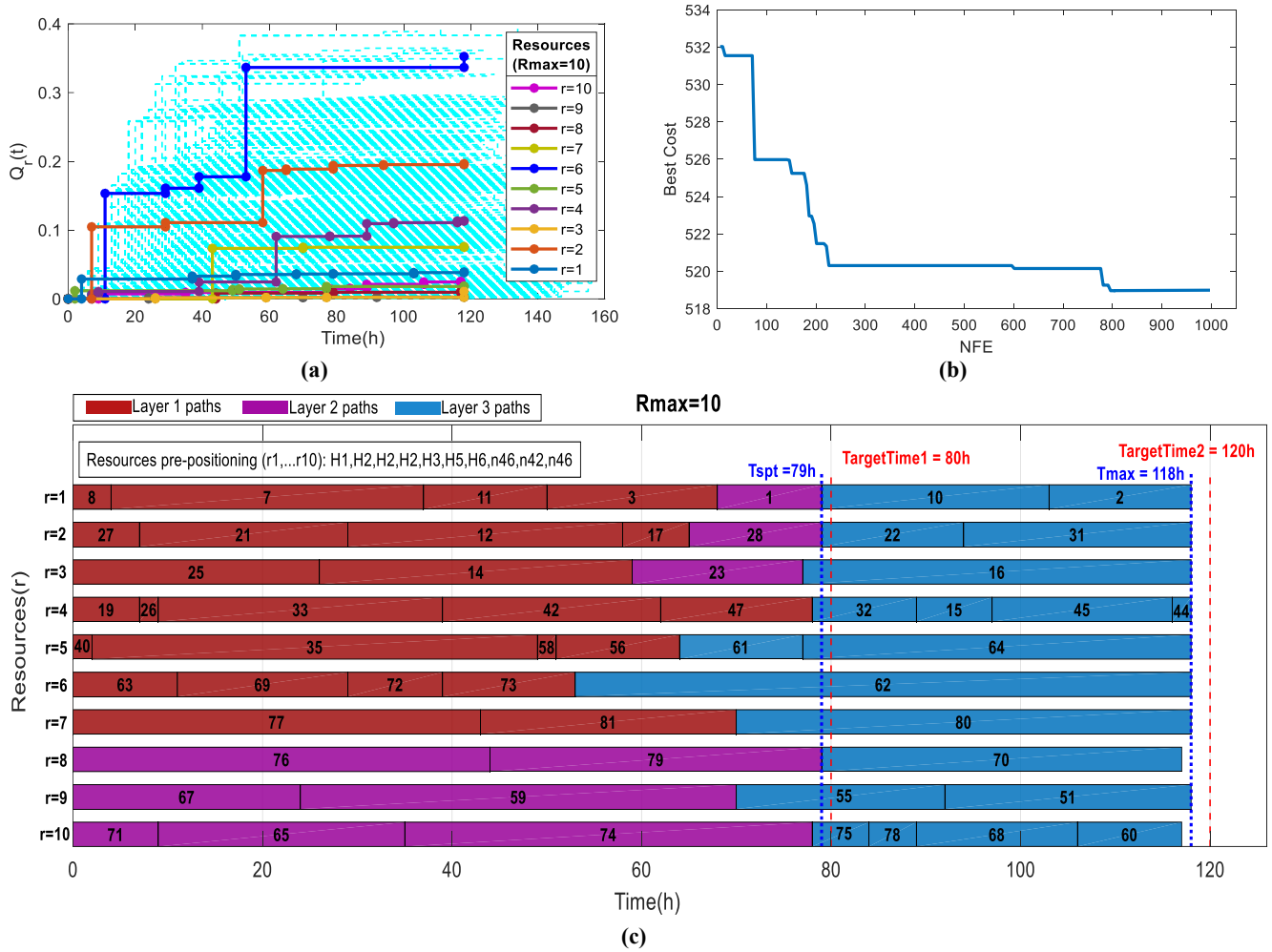

Fig.14: Network restoration optimization based on resilience (with 10 resources). (a) The functionality-time trajectories for network restoration and the optimal recovery, (b) Optimal cost with the number of function evaluations (NFE), (c) The optimal sequence for restoring blocked paths.

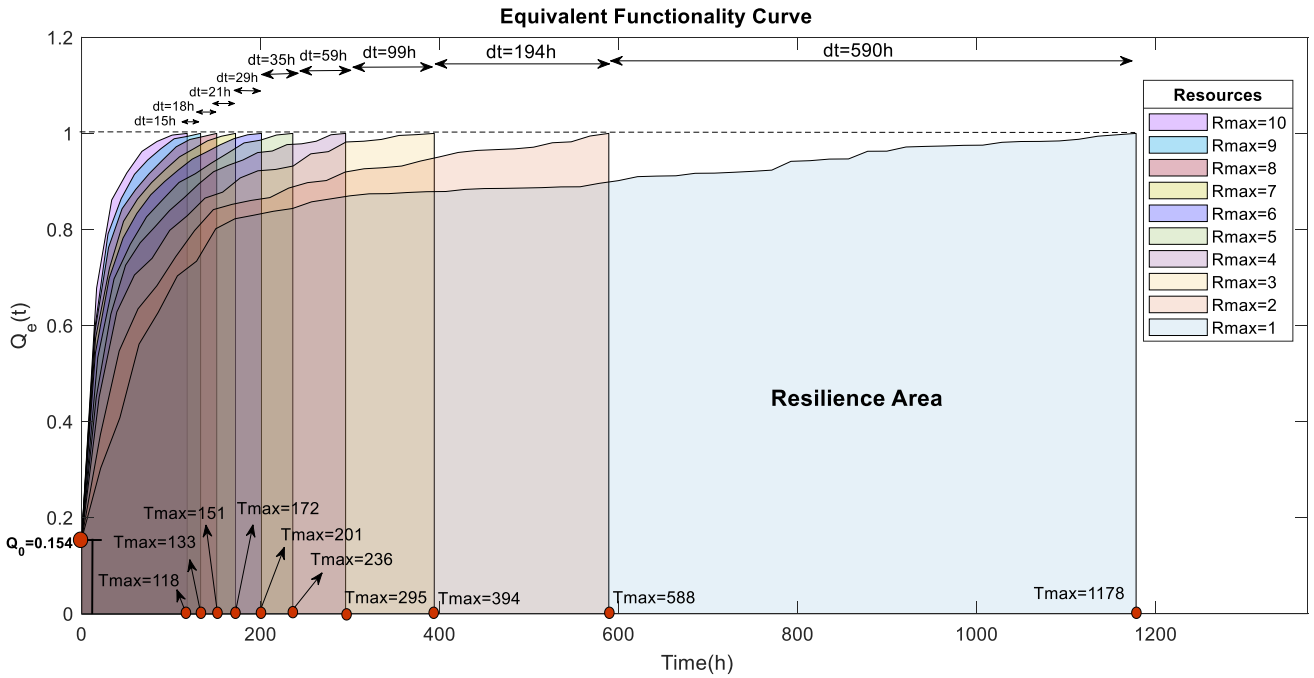

Fig. 15: Resilience of the network assessed through an equivalent functionality curve.

For every resource level, the functionality curves are set to reach a value of one at the end time (i.e. $Q_e(T_{max}) = 1$). This standardization facilitates a clear comparison of how varying numbers of resources affect the network's resilience and the optimal time for restoration. Figure 15 illustrates that with ten resources, network restoration is both quicker and more efficient, as shown by the resilience areas and completion duration (Tmax). Figure 15 shows that as more resources are added, the variation in completion durations (dt) diminishes. For instance, using two resources shortens the completion duration by 590 hours in comparison to one resource (i.e. $\Delta T_{max,R_{max}=1,2} = T_{max,R_{max}=1} - T_{max,R_{max}=2} = 1178 - 588 = 590h$), while adding a third resource further decreases the time by 194 hours in comparison to using two resources (i.e. $\Delta T_{max,R_{max}=2,3} = T_{max,R_{max}=2} - T_{max,R_{max}=3} = 588 - 394 = 194h$). In the end, adding a tenth resource has only shortened the completion duration by 15 hours in comparison to using nine resources. Figure 16 presents curves depicting the completion duration ratio $\left(\frac{(Tmax)_{R_{max}}}{(Tmax)_{R_{max}=1}}\right)$ and the resilience surface proportions $\left(\frac{S_{Rmax}}{S_{Rmax=1}}\right)$, clearly showing the influence of resource amount on network recovery time.

As can be seen in Figure 16, the completion time curve has converged at 0.1, indicating that the reduction in network restoration time is not significantly affected by adding more than 10 resources. As the result, as more resources are added, the variation in maximum completion times diminishes. In other words, the effectiveness of additional resources in shortening maximum completion times decreases.

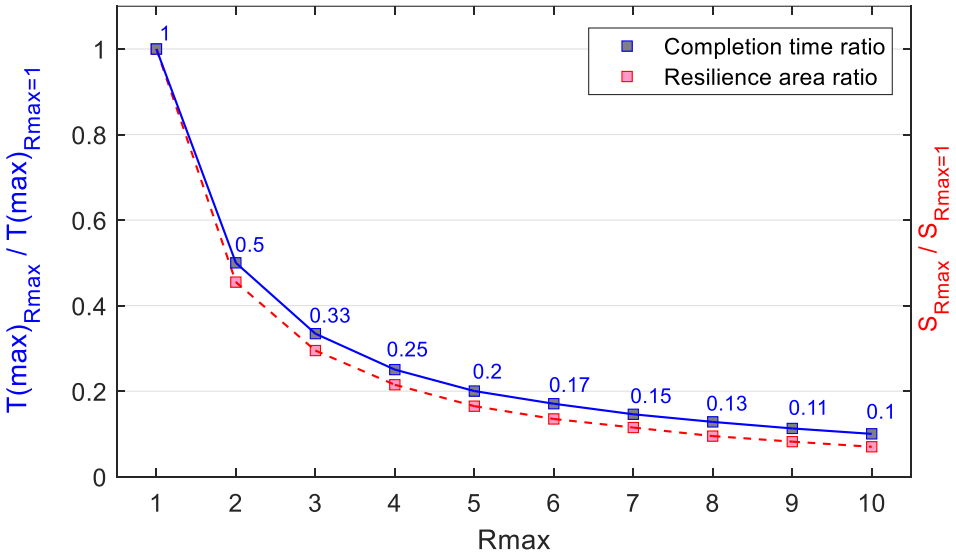

Fig. 16: The influence of the resources amount on recovery time and resilience area.

7. Conclusion

This study highlights the critical importance of seismic resilience in urban pathways, particularly in the context of building collapses following an earthquake. Through detailed analysis and modeling, we developed an optimized recovery plan that prioritizes the reopening of critical pathways to ensure rapid and effective emergency response. The proposed plan outlines the necessary resources and optimal sequence for debris removal and pathway restoration. Various probabilistic models were applied to simulate uncertainties in resilience assessments, including earthquake magnitude, epicenter location, structural damage, seismic intensity, debris, blockage, and evacuation. The mean of unblocking duration for every route serves as the ultimate outcome of probabilistic models. To optimize emergency resilience, a Simulated Annealing-based algorithm has been proposed. The proposed procedure has been implemented in a case study involving a transportation network in the Region 2 of Tehran metropolis, consisting of 51 nodes, 81 paths, and 6 emergency nodes. Desired durations for recovery have been set at 80 and 120 hours, respectively, and according to the calculations, ten resources are needed for network restoration. To investigate the influence of resource amount on network resilience, equivalent functionality curves have been developed. The equivalent curves demonstrated that using ten resources enables a rapid and efficient network recovery. It was shown that the impact of resource quantity on completion duration reduction diminishes with resource addition. The results indicate that the proposed methodology can be advantageous for optimizing emergency resilience and resource allocation in urban road networks. Our findings underscore that a proactive, well-coordinated recovery strategy significantly enhances the resilience of urban infrastructure, minimizing the disruption to emergency services and facilitating quicker recovery for affected communities.

References

[1] Lo, I.T., Lin, C.Y., Yang, C.T., Chuang, Y.J., Lin, C. H. (2020). Assessing the blockage risk of disaster-relief road for a large-scale earthquake. *KSCE J. Civ. Eng,* 24(12), 3820–3834. http://doi:10.1007/s12205-020-0340-7

[2] Yu, Y.C., Gardoni, P. (2022). Predicting road blockage due to building damage following earthquakes. Reliability Engineering & System Safety, 219, 108220. https://doi.org/10.1016/j.ress.2021.108220

[3] Tamima, U., Chouinard, L. (2017). Systemic seismic vulnerability of transportation networks and emergency facilities. J. Infrastruct.Syst, 23(4), 04017032. https://doi.org/10.1061/(ASCE)IS.1943-555X.0000392

[4] El-Maissi, A. M., Argyroudis, S. A., Kassem, M. M., Mohamednazri, F.(2023). Integrated seismic vulnerability assessment of road network in complex built environment toward more resilient cities. *Sustain Cities Soc*, 89, 104363. https://doi:10.1016/j.scs.2022.104363

[5] Anelli, A., Mori, F., Vona, M. (2020). Fragility curves of the urban road network based on the debris distributions of interfering buildings. *Appl. Sci.*, 10(4), 1289. https://doi:10.3390/app10041289

[6] Moya, L., Mas, E., Yamazaki, F., Liu, W., Koshimura, S. (2020). Statistical analysis of earthquake debris extent from wood-frame buildings and its use in road networks in Japan. *Earthq. Spectra*, 36(1), 209–231. https://doi:10.1177/8755293019892423

[7] Hirokawa, N., Osaragi, T. (2016). Tokyo Institute of Technology 2-12-1-W8-10, Ookayama, Meguro-ku, Tokyo 152-8550, Japan, 'Earthquake disaster simulation system: integration of models for building collapse, road blockage, and fire spread. *J. Disaster Res.*, 11(2), 175–187. https://doi:10.20965/jdr.2016.p0175

[8] Zanini, M. A., *et al.,*(2017). Post-quake urban road network functionality assessment for seismic emergency management in historical centres. *Struct. Infrastruct. Eng.*, 13(9), 1117–1129. https://doi:10.1080/15732479.2016.1244211

[9] Argyroudis, S., Selva, J., Gehl, P., Pitilakis, K. (2015). Systemic seismic risk assessment of road networks considering interactions with the built environment: Systemic seismic risk assessment of road networks. *Comput.-Aided Civ. Infrastruct. Eng.*, 30(7), 524–540. https://doi:10.1111/mice.12136

[10] Akbari, V., Sayarshad, H. R. (2022). Integrated and coordinated relief logistics and road recovery planning problem. *Transp. Res. Part Transp. Environ.* 111, 103433. https://doi:10.1016/j.trd.2022.103433

[11] García-Alviz, J., Galindo, G., Arellana, J., Yie-Pinedo, R. (2021). Planning road network restoration and relief distribution under heterogeneous road disruptions. *Spectr.* 43(4), 941–981. https://doi:10.1007/s00291-021-00644-x

[12] Pramudita, A., Taniguchi, E. (2014). Model of debris collection operation after disasters and its application in urban area. *Int. J. Urban Sci.*, 18(2), 218–243. https://doi:10.1080/12265934.2014.929507

[13] Nabavi, S. M., Vahdani, B., Nadjafi, B. A., Adibi, M. A. (2022). Synchronizing victim evacuation and debris removal: A data-driven robust prediction approach. *Eur. J. Oper. Res.* 300(2), 689–712. https://doi:10.1016/j.ejor.2021.09.051

[14] Briskorn, D., Kimms, A., Olschok, D. (2020). Simultaneous planning for disaster road clearance and distribution of relief goods: a basic model and an exact solution method. *Spectr.*, 42(3), 591–619. https://doi:10.1007/s00291-020-00589-7

[15] Shin, Y., Kim, S., Moon, I.(2019). Integrated optimal scheduling of repair crew and relief vehicle after disaster. *Comput. Oper. Res.*105. 237–247. https://doi:10.1016/j.cor.2019.01.015

[16] Maya, P. A., Dolinskaya, I. S., Sörensen, K. (2016). Network repair crew scheduling and routing for emergency relief distribution problem. *Eur. J. Oper. Res.* 248(1), 272–285. https://doi:10.1016/j.ejor.2015.06.026

[17] Shojaeian, A., Farahani, S., Behnam, B., Mashayekhi, M.R. (2021). Seismic Resilience Assessment of Tehran's Southern Water Transmission Pipeline Using GIS-based Analyses. *Numerical Methods in Civil Engineering*. 6(2), 93-106. 20.1001.1.23454296.2021.6.2.1.0

[18] Bruneau, M. et al. (2003). A Framework to quantitatively assess and enhance the seismic resilience of communities. *Earthq. Spectra*. 19(4), 733–752. https://doi:10.1193/1.1623497

[19] Haggag, M., Ezzeldin, M., El-Dakhakhni, W., Hassini, E. (2022). Resilient cities critical infrastructure interdependence: a meta-research. *Sustain. Resilient Infrastruct.* 7(4), 291–312. https://doi:10.1080/23789689.2020.1795571

[20] Cimellaro, G. P., Reinhorn, A. M., Bruneau, M. (2010). Seismic resilience of a hospital system. *Struct. Infrastruct. Eng.* 6(1–2), 127–144. https://doi:10.1080/15732470802663847

[21] Hosseini, S., Barker, K., Ramirez-Marquez, J.E., (2016). A review of definitions and measures of system resilience. Reliability Engineering and System Safety,145, 47-61, http://dx.doi.org/10.1016/j.ress.2015.08.006

[22] Atrachali, M., Ashtiany, M.G., Hosseini, K.A., Moghaddam, S.A. (2019). Toward quantification of seismic resilience in Iran: Developing an integrated indicator system. International Journal of Disaster Risk Reduction, 39. https://doi.org/10.1016/j.ijdrr.2019.101231

[23] Poulin, C., Kane, M.B. (2021). Infrastructure resilience curves: Performance measures and summary metrics.

Reliability Engineering and System Safety. 216, 107926. https://doi.org/10.1016/j.ress.2021.107926

[24] Bocchini, P., Frangopol, D.M., Ummenhofer, T., Zinke, T. (2014). Resilience and sustainability of civil infrastructure: Toward a unified approach. Journal of Infrastructure Systems. 20(2).
https://doi.org/10.1061/(ASCE)IS.1943-555X.0000177

[25] Ahmadian, N., Lim, G.J., Cho, J., Borac, S. A. (2020). quantitative approach for assessment and improvement of network resilience. Reliability Engineering and System Safety.200,106977. https://doi.org/10.1016/j.ress.2020.106977

[26] Mahsuli, M., Haukaas, T. (2013). Seismic risk analysis with reliability methods, part I: Models. Structural Safety,42,54–62.
https://doi.org/10.1016/j.strusafe.2013.01.003

[27] Alavi, S.H., Bahrami, A., Mashayekhi, M., Zolfaghari, M. (2024) Optimizing interpolation methods and point distances for accurate earthquake hazard mapping. *Buildings*, 14(6), 1823.https://doi.org/10.3390/buildings14061823

[28] Hosseini, Y., Mohammadi, R. K., Yang, T. Y. (2023). Resource-based seismic resilience optimization of the blocked urban road network in emergency response phase considering uncertainties. *Int. J. Disaster Risk Reduct.* 85, 103496. https://doi.org/10.1016/j.ijdrr.2022.103496

[29] Hosseini, Y., Mohammadi, R. K., Yang, T. Y. (2024). A comprehensive approach in post-earthquake blockage prediction of urban road network and emergency resilience optimization. *Reliability Engineering and System Safety.* 244, 109887. https://doi.org/10.1016/j.ress.2023.109887

[30] Darzi, A., Zolfaghari, M. R., Cauzzi, C., Fäh, D. (2019). An empirical ground-motion model for horizontal PGV, PGA, and 5% damped elastic response spectra (0.01–10 s) in Iran. *Bull. Seismol. Soc. Am.* 109(3), 1041–1057. https://doi:10.1785/0120180196

[31] Fallah Tafti, M., Amini Hosseini, K., Mansouri, B. (2020). Generation of new fragility curves for common types of buildings in Iran. *Bull. Earthq. Eng.*18(7), 3079–3099. https://doi:10.1007/s10518-020-00811-5

[32] Anastassiadis, A. J., Argyroudis, S. A. (2007). Seismic vulnerability analysis in urban systems and road networks. Application to the city of Thessaloniki, Greece. *Int. J. Sustain. Dev. Plan.* 2(3), 287–301.
https://doi:10.2495/SDP-V2-N3-287-301

[33] D'Agostino, G., et al.(2019). Earthquake simulation on urban areas: improving contingency plans by damage assessment', in *Critical Information Infrastructures Security*, (Lecture Notes in Computer Science) Cham: Springer International Publishing. 11260, 72–83.
https://doi:10.1007/978-3-030-05849-4_6

[34] Cormen,T. H., Leiserson, C. E., Rivest, R. L. and Stein, C. (2022) Introduction to algorithms, fourth edition. The MIT Press, Cambridge, Massachusetts London, England.

[35] Zafarani, H., Noorzad, A., Ansari, A., Bargi, K. (2009). Stochastic modeling of Iranian earthquakes and estimation of ground motion for future earthquakes in Greater Tehran. Soil Dynamics and Earthquake Engineering. 29, 722-741. https://doi.org/10.1016/j.soildyn.2008.08.002

[36] Feng, C.M., Wang, T.C. (2003). Highway emergency rehabilitation scheduling in post-earthquake 72 Hours. Journal of the Eastern Asia Society for Transportation Studies, 5.